NIH Public Access
Author Manuscript
Nat Immunol. Author manuscript; available in PMC 2006 September 5.

Published in final edited form as:
Nat Immunol. 2005 July ; 6(7): 707–714.

Stable T cell-dendritic cell interactions precede the development of both tolerance and immunity *in vivo*

Guy Shakhar[1,*], **Randall L. Lindquist**[2,*], **Dimitris Skokos**[2], **Diana Dudziak**[2], **Julie H. Huang**[1], **Michel C. Nussenzweig**[2,3,#], and **Michael L. Dustin**[1,#]

1 *Program in Molecular Pathogenesis and Department of Pathology, Skirball Institute of Biomolecular Medicine, New York University School of Medicine, New York, NY 10016 USA*

2 *Laboratory of Molecular Immunology,*

3 *Howard Hughes Medical Institute, The Rockefeller University, New York, NY 10021 USA.*

Abstract

The maturation status of dendritic cells (DCs) determines whether they prime or tolerize T cells. We targeted ovalbumin peptide exclusively to DCs *in situ* using an antibody against DEC-205 and studied DC interaction with naïve $CD4^+$ T cells under tolerizing or priming conditions. Two-photon microscopy was used to simultaneously track antigen-specific OT-II T cells, non-specific T cells and DCs in lymph nodes of living mice. In both tolerance and immunity, OT-II cells arrested on DCs near high endothelial venules beginning shortly after extravasation and regained their baseline speed by 18 h. Thus, early antigen-dependent T cell arrest on DCs is a shared feature of tolerance and priming associated with activation and proliferation.

Laser scanning microscopy allows imaging of live cells at a depth of up to 300 μm in lymph nodes removed from mice (explanted) [1–6] or exposed surgically in anesthetized mice (intravital)[7–9]. Both kinds of preparations have been used to study mature DCs actively participating in immune responses[1,3–5,7], but lymph nodes imaged by intravital microscopy differed from the explanted preparations in preserving blood and lymph flow.

Mature DCs have been visualized by labeling with exogenous fluorescent dyes and were found to crawl slowly in random directions, rapidly extending and retracting long dendritic processes[1,3–5,7]. We have examined the behavior of steady state DCs in live anesthetized mice by intravital 2-photon microscopy CD11c-EYFP transgenic mice that express high amounts of enhanced yellow fluorescent protein (EYFP) in $CD11c^+$ DCs[10]. DCs in these mice are indistinguishable from DCs of wild-type mice based on immunohistochemistry and flow cytometry. In the steady state, DCs actively probed passing T cells with dendritic processes, but showed little translational movement and were found in extensive interdigitating networks within the T cell zones. These DCs networks were present throughout the T cell area, including around High endothelial venules (HEVs), such that T cells exiting HEVs would encounter the DC network rapidly. In addition, we noted that transferred mature DCs displayed translational movement as they dispersed throughout the networks of endogenous DCs[10].

The outcome of antigen presentation by DCs depends on the state of DC differentiation or maturation[11–16]. In the steady state, immature DCs capture, process, and present to T cells a variety of self and environmental antigens including proteins from serum, commensal

Correspondence and requests for materials should be addressed to Michael L. Dustin (212) 263-3207 (phone) (212) 263-5711 (fax) dustin@saturn.med.nyu.edu Or Michel C. Nussenzweig (212)-327-8067 (phone) (212) 327-8370 (fax) nussen@mail.rockefeller.edu.
* and # signify equal contribution

Competing interests statement The authors declare that they have no competing financial interests.

NIH-PA Author Manuscript
NIH-PA Author Manuscript
NIH-PA Author Manuscript

NIH-PA Author Manuscript

NIH-PA Author Manuscript

NIH-PA Author Manuscript

microbes, and dead cells[17–22]. Presentation of agonistic peptides on major histocompatibility complex (MHC) by steady state DCs tolerizes T cells and prevents autoreactivity when the same antigens are subsequently presented under immunizing conditions[16,23–27]. In contrast, DCs activated to mature by inflammatory stimuli, including infection, Toll-like receptor ligands, and CD40 ligation, induce strong effector T cell responses to the same antigens[11–16,23,24,28–30].

Intravital two-photon microscopy was used to image T cell priming in lymph nodes[7], and showed that T cells interact with fully mature, antigen-loaded, DCs in 3 phases. For the first 8 h, T cells transiently contacted DCs, between 8–20 h they established stable contacts, and finally resumed dynamic movement. In contrast, when tolerance was examined in explanted lymph nodes[6], T cells did not establish prolonged contacts with antigen-loaded DCs. These differences in early T cell migration suggests that the stability of T cell-DC interactions determines commitment to tolerance or immunity[6]. However, non-specific control T cells were not simultaneously visualized, and experiments based on classical immunological methods indicate that the early stages of T cell-DC interactions are similar in tolerance and priming[23,24,27,31,32] and do not commit T cells to either [33].

To examine tolerance and immunity in live mice, we developed a method for visualizing endogenous DCs simultaneously interacting with antigen-specific and non-specific $CD4^+$ T cells. This allowed us to control for the variability in T cell movement within different sub-compartments of the lymph node. Here we report a novel antigen-specific stop signal that acts within an hour of T cells leaving the HEVs in both immunity and tolerance.

RESULTS

Antigen delivery by α-DEC-205

We sought to determine how widely divergent endpoints of tolerance and immunity relate to the physical interaction between DCs and $CD4^+$ T cells during early stages of antigen recognition. To deliver antigen to DCs *in vivo*, we injected mice with α–DEC-OVA, a recombinant monoclonal antibody against DEC-205 engineered[23] to carry an in-frame C-terminal peptide (amino acids 323–339) from ovalbumin. $CD4^+$ OT-II T cells recognize this peptide when it is presented by $I\text{-}A^{b}$[34]. To compare conditions of tolerance to priming we used α-CD40 as an adjuvant. α–CD40 is the only single-component adjuvant that we have examined that induces long-lived effector T cells with a single injection[30]. α-CD40 induced upregulation of CD80, CD86 and MHC class II on lymph node $CD11c^+$ DCs between 6 and 12 h after injection (Supplementary Fig. 1 on-line). Accordingly we timed α-CD40 injection such that upregulation of CD80, CD86 and MHC class II were maximal in the time frame of our imaging experiments.

In the steady state (no α–CD40) OT-II cells responded to α–DEC-OVA by up-regulating CD69 and down-regulating CD62L surface expression within 3 h of exposure to antigen (Fig. 1a). By day 3 there was extensive T cell division, but most of the responding cells were deleted by day 7 (Fig. 1b,c). Whereas OT-II cells re-isolated after 3 days remained antigen responsive, the few OT-II cells remaining after 7 days were unresponsive to re-stimulation *in vitro* and therefore tolerant (Fig. 1d). When α-CD40 was given in conjunction with α–DEC-OVA, similar expression of CD69 and CD62L was found and similar amounts of OT-II cell division were seen at day 3 (Fig. 1a). However, OT-II cells responding to antigen in the presence of α-CD40 adjuvant persisted at day 7 and showed enhanced proliferation in response to antigen *in vitro*, indicating T cell priming (Fig. 1b,c,d). Thus, antigen presentation by DCs targeted with α–DEC-OVA resembles previously described α–DEC targeted antigens in that the outcome of antigen presentation in the steady state differs dramatically from presentation of the same antigen under immunizing conditions[23,24,27,30]. Therefore, despite the difference

NIH-PA Author Manuscript

NIH-PA Author Manuscript

NIH-PA Author Manuscript

in outcome, T cells responding to antigen presented by DCs under tolerizing and immunizing conditions are initially (day 3) indistinguishable in terms of cell surface activation antigen expression and ability to respond to antigen *in vitro*.

T cell retention around HEVs

To determine whether T cells were differentially distributed in lymph nodes under conditions of tolerance and immunity, we examined the fate of EGFP-expressing antigen-specific ($CD4^+$ OT-II T cells) and non-specific T cells (naïve non-TCR transgenic $CD4^+$ T cells) in lymph nodes at 3 or 24 h after exposure to antigen. At 3 h post-transfer, antigen-specific T cells were found in close proximity to HEVs (average distance of 59 μm), and only 13% of them were in the deep paracortex (Fig. 2). In contrast, the non-specific T cells were an average of 78 μm from HEVs ($p<0.0001$), and were more evenly distributed throughout the T cell area, with 32% in the deep paracortex. By 24 h, both specific and non-specific cells were uniformly distributed throughout the T cell area with 43–45% present in the deep paracortex, and were located on average 90 μm from the center of the nearest HEV (Fig. 2). CD40 ligation did not alter the distribution of either the antigen-specific or non-specific T cells at either time point (Fig. 2). Similar experiments simultaneously visualizing enhanced cyan fluorescent protein-expressing (ECFP) OT-II cells and EGFP-expressing non-specific T cells showed identical results (data not shown). We conclude that T cells that recognize specific antigen are restricted to the area around HEVs in the early phases of tolerogenic and immunogenic responses.

Visualizing DCs and T cells in live mice

To visualize interactions between DCs and T cells, we injected CD11c-EYFP mice[10] with α-DEC-OVA with or without α-CD40 (Supplementary Fig. 2 on-line); five h later, we adoptively transferred ~10^7 antigen-specific EGFP-OT-II cells and an equal number of naïve control non-TCR transgenic $CD4^+$ ECFP-T cells. In some experiments blood vessels were identified by injection of Q-dots (quantum dots coated with polyethylene glycol, Supplementary Video 1 on-line). All fluorescent cell types were simultaneously imaged in anaesthetized mice, at multiple depths (10 to 200 μm) including the outer paracortex near HEVs to the deep paracortical T cell zones up to 18 h after T cell transfer (Fig. 3b). T cells extravasated in the first hour after injection, and few extravasation events were observed during the imaging period (Supplementary Video 2 on-line). Although other groups described depth as a critical determinant of T cell motility[7,35], we found little correlation between depth and cell speed (Supplementary Fig. 3 on-line).

$EYFP^+$ DCs present in the imaging fields sensitively indicated the viability of the preparation. By simultaneously visualizing OVA-specific EGFP-OT-II cells, non-specific ECFP-T cells and EYFP DCs in each field, we could identify immobility caused by phototoxicity, suboptimal temperature, inadequate blood supply or surgical trauma. Fields in which T cells were globally arrested and DCs stopped probing were excluded from analysis (Supplementary Video 3 on-line). Cells were tracked in three dimensions over the course of each imaging experiment, and T cell motility was quantified with regard to velocity (Fig. 4, Supplementary Figs. 4 and 5 on-line), immobility (Fig. 5), and directionality (Fig. 6). Overall, 2100 cell tracks from 62 imaging fields in 29 mice were included in our final analysis.

Tolerance *in vivo*

We found that tolerance was associated with early T cell immobility followed by recovery over a period of 6–12 h. One to 6 h after injection with α-DEC-OVA (Figs. 3, 4, Supplementary Figs. 4, 5 on-line, Supplementary Video 4 on-line), antigen-specific EGFP-OT-II T cells moved significantly more slowly than non-specific ECFP-T cells (mean velocity, 4.41 vs. 9.41 μm/min, $p< 0.0005$, Fig. 4). A large proportion of the specific T cells were immobile (slower than 2 μm/min) in this interval (35% vs. 8.7% specific vs. non-specific T cells $p<0.0001$, Fig. 5a),

NIH-PA Author Manuscript

NIH-PA Author Manuscript

NIH-PA Author Manuscript

and many sessile antigen-specific cells were found just outside HEVs (Fig. 2d, Supplementary Video 5 on-line). In addition to immobility we measured the arrest coefficient[6], which is the proportion of time that a T cell is arrested (instantaneous velocity < 2 μm/min). Antigen-specific T cells spent more time arrested than did control cells (47% vs. 20%, $p<0.0001$, Fig. 5b). To determine the directionality of T cell movement, we measured the turning angle[7] and confinement index[6] (see Methods). Consistent with their relative immobility, we found that antigen-specific T cells moved less linearly than non-specific cells, as evidenced by a higher turning angle (82° vs. 61°, $p<0.0001$, Fig. 6a) and a lower confinement index (41% vs. 56%, $p<0.0001$, Fig. 6b). In the 6–12 h interval (Supplementary Video 6 on-line), the specific T cells remained significantly slower than the non-specific T cells (5.94 vs. 7.46 μm/min, $p<0.0001$, Fig. 4), but the specific T cells were moving faster than in the 1–6 h interval (5.94 vs. 4.41 μm/min, $p<0.001$, Fig. 4). Between 6 and 12 h, antigen-specific T cells were more immobile (12.2% vs. 6.0%, $p<0.05$, Fig. 5a), had larger arrest coefficients (32% vs. 13%, $p<0.0001$, Fig. 5b) and smaller confinement index (53% vs. 66%, $p<0.0001$, Fig. 6b) than the non-specific T cells. Finally, at 12–18 h (Supplementary Video 7 on-line), the antigen-specific T cells were still significantly slower (7.05 vs. 8.83 μm/min, $p<0.0001$, Fig. 4), more immobile (12% vs. 2.8%, $p<0.002$, Fig. 5a) and had higher arrest coefficients (32% vs. 22.3%, $p<0.001$, Fig. 5b) than control T cells, but differences in the turning angle and confinement index were not significant (Fig. 6). Two-way analysis of variance (ANOVA) showed that the speed difference between antigen-specific and non-specific cells was significantly greater at 1–6 h than at either 6–12 or 12–18 h ($p<0.0001$ for both), whereas the difference at 6–12 h was statistically indistinguishable from the difference at 12–18 h. This suggests that antigen-specific cells were regaining motility at 6–12 h. We conclude that T cells exposed to antigen under tolerizing conditions arrest near HEVs, and that mobility recovers significantly by 6–12 h after antigen exposure.

To determine whether the difference in T cell speeds reflects the induction of antigen-specific tolerance or inherent differences between EGFP-OT-II cells and ECFP-T cells, we examined the behavior of EGFP-OT-II cells under control conditions. Mice were injected with an irrelevant peptide targeted to DEC-205 (α-DEC-CSP) or with OVA peptide fused to an isotype-control antibody (Iso-OVA). Under both conditions, EGFP-OT-II cells moved at around 9 μm/min, a speed comparable to those of the non-specific ECFP-T cells in α-DEC-OVA treated mice (data not shown) and to those reported previously[2–5,7,8]. Thus, the arrest of EGFP-OT-II cells in mice treated with α-DEC-OVA was antigen-specific.

Priming *in vivo*

As in tolerance, immunity was associated with an early antigen-specific arrest of T cells, but recovery to normal movement was somewhat slower (Fig 4, Supplementary Figs. 4, 5 online). In mice treated with α-DEC-OVA and α-CD40 (Supplementary Video 8 on-line), specific EGFP-OT-II T cells moved significantly slower than non-specific ECFP-T cells in the 1–6 h interval (mean velocity, 5.20 vs. 8.78 μm/min, $p<0.0001$, Fig. 4). In this interval the specific T cells were more immobile (31% vs. 9.6%, $p<0.0001$, Fig. 5a), had a higher arrest coefficient (40% vs. 21%, $p<0.0001$, Fig. 5b), a sharper turning angle (71% vs. 61%, $p<0.05$, Fig. 6a) and a smaller confinement index (41% vs. 49%, $p<0.02$, Fig. 6b) than non-specific T cells. In the 6–12 h interval (Supplementary Video 9 on-line), specific T cells remained slower than non-specific cells (4.35 vs. 8.05 μm/min, $p<0.0001$, Fig. 4), had a higher arrest coefficient (46% vs. 27%, $p<0.0001$, Fig. 5b), but were no longer significantly more immobile (Fig. 5a). They displayed a smaller confinement index (40% vs. 49%, $p<0.02$, Fig. 6b), but showed no significant difference in turning angle (Fig. 6a). Finally, in the 12–18 h interval (Supplementary Video 10 on-line), specific T cells moved slightly slower (6.08 vs. 7.54 μm/min, $p<0.005$, Fig. 4), and had slightly higher arrest coefficient (35% vs. 28%, $p<0.05$, Fig. 5b) than non-specific cells, but were otherwise indistinguishable. Two-way ANOVA showed that the speed

NIH-PA Author Manuscript

NIH-PA Author Manuscript

NIH-PA Author Manuscript

difference between antigen-specific and non-specific cells was significantly smaller at 12–18 h than at 1–6 h ($p<0.003$) and 6–12 h ($p<0.006$), while the difference at 1–6 h was statistically indistinguishable from the difference at 6–12 h. We conclude that under conditions of immunity, specific cells arrest initially and then recover mobility significantly 12–18 h after antigen exposure. Occasionally, we observed discrete T-DC clusters forming around DCs (Supplementary Video 11 on-line), but T cells were not always in clear contact with $CD11c^{hi}$ DCs (Supplementary Video 12 on-line), perhaps because not all $DEC\text{-}205^{+}$ cells express high amounts of EYFP in CD11c-EYFP transgenic mice[10].

Comparison of tolerance and priming *in vivo*

Tolerance and immunity were similarly characterized by an early arrest followed by restoration of mobility. This was also seen when the speed of antigen-specific T cells was normalized to that of in-field non-specific control cells (Supplementary Fig. 5 on-line). Overall, there was little evidence for perturbation of control T cells, which maintained their mobility for at least 18 h. The most revealing parameter for comparison of specific cells under conditions of tolerance and immunity was the arrest coefficient[6], a continuous parameter reflecting the percentage of time T cells were arrested (Fig. 5b). At 1–6 h the arrest coefficient for specific T cells was slightly higher under conditions of tolerance than immunity (47% vs. 40%, $p<0.02$). In contrast, at 6–12 the arrest coefficient was higher in immunity (32% vs. 46%, $p<0.005$). Finally, at 18 h the arrest coefficients were uniform (32% vs. 35%, n.s.). Over the entire 1–18 h period the average arrest coefficient for antigen-specific cells was similar for both conditions (~38%), as was the average cell speed (5.7 vs. 5.4 μm/min, n.s.). We conclude that while there were small differences in the dynamics of specific T cell DC interactions in tolerance and immunity, the trend of early arrest and slow recovery over 18 h was similar.

DISCUSSION

Our results show that OVA-specific T cells slowed down and exhibited confined motion upon encountering antigen, many of them arresting in the vicinity of HEVs. Meanwhile, the non-specific cells in the same field maintained their baseline speed and directionality. The early arrest near HEVs was identical in conditions of tolerance and priming, but antigen-specific T cells regained mobility more rapidly under conditions of tolerance than priming.

Intravital imaging of lymph nodes in mice injected with mature antigen-loaded DCs, showed that naïve T cells interacted with DCs in three stages: during the first 8 h, or phase 1, T cells interact with antigen-bearing DCs dynamically with no prolonged stopping, T cell immobility was seen between 8–20 h, or phase 2, and motility recovered thereafter in phase 3[7]. Similar kinetics were observed in explanted lymph nodes when antigen was delivered by migrating mature DCs[5]. It was suggested that transient T-DC interactions in phase 1 changed the T cell activation state so that it could undergo stable interactions in phase 2[7,36]. Although our finding that T cells stop shortly after leaving the HEVs was surprising in this light, it was independently supported by histological evidence showing preferential retention of antigen-specific T cells around HEVs, which indicated constrained movement. Our results agree with previous work showing histologically that immunization with complete Freund's adjuvant resulted in early antigen-dependent retention of T cells near HEVs[37]. Furthermore, *in vitro* experiments show that T cells stop migrating immediately upon exposure to their cognate antigen[38,39]. Steady-state lymph node DCs express high amounts of MHC class II and intermediate amounts of CD80 and CD86[10,40]. Therefore, the rapid arrest we observe under tolerogenic conditions *in vivo* is not inconsistent with *in vitro* observations of poor immunological synapse formation in the absence of costimulation[41,42]. We conclude that a prolonged period of transient interactions is not necessary to form stable conjugates between T cells and DCs. Potential explanations for the differences in the length of phase 1 between ours and previous studies

NIH-PA Author Manuscript

NIH-PA Author Manuscript

NIH-PA Author Manuscript

include their use of exogenously administered DCs that must migrate to the lymph node, and enter the T cell area before presenting antigen[7]. Another possibility is that T cells integrate signals during phase 1 encounters with DC. In this model, antigen presented by many DCs after DEC-205 targeting[43,44] might produce an integrated signal of the same magnitude as that obtained by T cells interacting with much less frequent immigrant DCs for 8 h. While further experimentation is needed to test these possibilities, it is likely *a priori* that the number of antigen-positive DCs will vary depending upon how antigen reaches the lymph node. For example, soluble antigen rapidly drains to the lymph nodes and is widely accessible to resident lymph node DCs[45]. In addition, self-antigens from dead cells and serum proteins are continually picked up, processed and presented by large numbers of resident DCs in the steady state. Thus, it seems likely that under conditions of immunity or tolerance, T cells can encounter varying numbers of antigen-bearing DCs, and that the kinetics of the initial T cell-DC interaction will depend on the relative frequency of antigen-positive DCs.

Imaging of T cell priming in explanted lymph nodes showed antigen-specific T cell clustering around DCs in the deep paracortex[3,6]. We rarely observed formation of discrete T-DC clusters but this was expected, as large numbers of DEC-205$^+$ DCs in the lymph node present antigen after targeting with the α-DEC-OVA antibody[23,30], and the number of T cells in each cluster is inversely proportional to the number of antigen presenting DCs[3]. In our experiments, arrested antigen-specific T cells were not always in clear contact with CD11c^{hi} DCs, which is consistent with the partial overlap between EYFP and DEC-205 expression in CD11c-EYFP Tg mice[10].

We found that the early stages of tolerance and immunity were similar in terms of T cell arrest near HEVs at 1–5 h followed by resumed movement and dispersion in the deep paracortex by 18 and 24 h, respectively. The only difference observed was that return to rapid migration was slower under conditions of priming than tolerance. Our imaging experiments are consistent with our finding that T cell activation markers are identical and proliferation and responses to antigen *in vitro* are similar in the first 3 days of priming and tolerance induction. These experiments are also in agreement with physiologic studies showing that T cells activated by soluble peptide *in vivo* are not committed to tolerance after 3 days[31–33]. Our results differ from an earlier two-photon study of tolerogenic T-DC interactions which used the same antigen delivery method (α–DEC-205-OVA)[6]. This study reported that CD8$^+$ T cell arrest exclusively in priming and not in tolerance. However, these experiments were performed in explanted lymph nodes where DCs were labelled by direct lymph node injection of anti-CD11c, and non-specific T cells were not simultaneously imaged[6]. Importantly, our use of intravital microscopy preserves blood and lymph flow whereas these physiological processes were lacking in the explanted lymph nodes used previously[6].

What is the significance of the prolonged T cell-DC interactions early in immune responses? Our experiments suggest that these conjugates are antigen-specific, but not associated with commitment to immunity or tolerance and independent of the state of DC maturation. We speculate that stable contacts between DCs and T cells are an integral part of initial T cell activation *in vivo*, and that commitment to immunity or tolerance occurs later as T cells dynamically contact DCs.

Methods

Transgenic mice

EYFP-CD11c mice, described previously[10] express EYFP-Venus under the control of the CD11c promoter, and exhibit bright fluorescence specifically in dendritic cells. EGFP-OT-II transgenic mice were products of a cross between OT-II mice and mice ubiquitously expressing EGFP on the β-actin promoter[46,47]; ECFP-OT-II mice are a cross between mice expressing

NIH-PA Author Manuscript

NIH-PA Author Manuscript

NIH-PA Author Manuscript

ECFP on the β-actin promoter from Jackson Labs[48] and OT-II mice. All strains used are fully backcrossed to a C57Bl/6 background. Mice were used for experiments at the age of 4–6 weeks; all mice were housed under SPF conditions and treated in accordance with IACUC protocols of Rockefeller and New York universities.

Immunofluorescence

Lymph nodes were fixed in PBS with 4% paraformaldehyde + 10% sucrose and cryoprotected in PBS + 30% sucrose before embedding in OCT and freezing. Frozen tissue was sectioned on a microtome and fixed in acetone. All incubations were performed in a humidified chamber. Sections were blocked in 5% BSA, 10% serum in PBS in the presence of α-CD16/CD32 (BD Biosciences), and sequentially blocked with excess streptavidin and biotin (Vector Labs). The antibodies used were: directly labeled α-CD3ε-Alexa 647, α-B220-Alexa 647 (CalTag), biotinylated α-rat IgM, and unconjugated MECA-79 (BD Biosciences). Streptavidin-Cy3 was from Jackson ImmunoResearch. Sections were mounted in Fluoromount-G (Southern Biotech) and stored at 4 °C.

Confocal microscopy

Confocal images were acquired on a Zeiss LSM 510 system with 405, 488, 543, and 633 nm excitation lines; EGFP and ECFP fluorescence were visualized directly in all images. An array of 40x images was taken with a motorized stage to capture the entire cut surface of the lymph node, and images were exported into Adobe Photoshop for final processing. Positions of T cells, HEVs, and the deep paracortex were measured in Volocity software. Cells were scored as being in the deep paracortex only if the entire cell was within the boundary; cells touching the boundary were excluded. The minimum distance from T cells to HEVs were calculated as described elsewhere[37] with the following equation: $D_i = \min\sqrt{[(x_i - x_j)^2 + (y_i - y_j)^2]}$, where i and j are indices from 1…n for T cells and HEVs, respectively, and min is the minimum function. It should be noted that this yields the distance to the center of the HEV, which is greater than the distance to the basal side of the HEV endothelium.

Recombinant Antibodies

α–DEC-OVA, and α-DEC-CSP (anti-DEC-205 fused to the irrelevant peptide SYVPSAEQI) were produced by replacing the HEL peptide-encoding sequence in α-DEC-HEL[23] by molecular cloning. Iso-OVA was prepared as described previously[23]. Recombinant antibodies were produced by transient transfection and purified as previously described[23].

Antigen Delivery and Cell Transfer

CD11c-EYFP mice were injected i.p. with 2 μg of α-DEC-OVA, Iso-OVA or α-DEC-CLS either alone or together with α-CD40 (clone 1C10, 50 μg). Five h later mice were injected i.v. with 1–2 × 10^7 purified EGFP-OT-II cells and naïve $CD4^+$ ECFP-T cells (>98% purity) prepared by magnetic depletion of non-$CD4^+$ T cells (MACS $CD4^+$ T cell Kit, Miltenyi Biotec). Lymph nodes were imaged 2–18 h after T cell transfer (Fig. 3a). To examine HEVs *in vivo*, we injected 10 μg of Alexa 594-labeled MECA-79 antibody i.v.

Transgenic T cell responses

OT-II T cells (CD45.2) were labeled with CFSE, transferred into 4 to 6 week-old B6/SJL mice and challenged i.p. 24 h later with 2 μg of α-DEC-OVA, 2 μg Iso-OVA, PBS, or 2 μg α-DEC-OVA plus 90 μg α–CD40. T cells were purified from peripheral lymph nodes 3 d or 7 d later and either cultured with irradiated $CD11c^+$ cells and OVA peptide to measure proliferation or analyzed by flow cytometry on a FACSCalibur (BD Pharmingen) to measure CFSE dye dilution (gated on $V\alpha_2$ and CD45.2). To monitor early T cell activation, CD45.2 OT-II T cells

NIH-PA Author Manuscript

NIH-PA Author Manuscript

NIH-PA Author Manuscript

were transferred into CD45.1 B6/SJL mice injected with α-DEC-OVA (with or without α-CD40) five h previously; T cells were purified from lymph nodes at 3, 12, or 24 h after T cell transfer and analyzed by flow cytometry to measure surface expression of CD69 and CD62L (gated on $V\alpha_2$ and CD45.2). Antibodies were from BD Pharmingen.

Surgery

Mice were anaesthetized with 100 mg ketamine, 15 mg xylazine and 2.5 mg acepromazine per kg, and kept anaesthetized with hourly injections of half this dose. Mice were restrained on a stage warmer at 37 ºC (BioTherm Micro S37, Biogenics) and the abdominal skin was incised from the edge of the rib cage through the midline to the thigh. A skin flap was separated from the abdominal muscle to expose the inguinal lymph node..

To stabilize, moisturize and maintain the lymph node at 37 ºC, we placed the skin flap on a thermoconductive base made of silicone elastomer (Sylgard 184, Dow Corning) surrounding a core of thermoconductive putty (T-putty 502, Thermagon). The connective and adipose tissue covering the lymph node was removed by microsurgery keeping blood and lymph vessels intact, and a saline filled chamber consisting of a cover-slip glued to a nylon washer was mounted on the skin flap over the lymph node. The chamber was laterally secured by 3 insect pins piercing the skin and lodged in the silicone base. The temperature was monitored using a probe (Bioptechs) placed near the lymph node to ensure that it was at 37±1 ºC. To compensate for anesthesia-induced respiratory depression, we provided mice with 100% oxygen by mask throughput the imaging session.

Intravital microscopy

The lymph node was imaged using a Bio-Rad Radiance multiphoton microscope fitted with a Tsunami pulsed laser (Spectraphysics) and controlled by Lasersharp2000 software (Bio-Rad) We used a Nikon 40× objective (water immersed, NA 0.8). To image EYFP, EGFP and ECFP, the excitation wavelength was set to 910 nm. Band-pass filters optimized for detecting EYFP (550/30) and ECFP (510/30) and a 530 long-pass dichroic mirror were used to detect fluorescent proteins, with EGFP bright in both channels. Polyethylene glycol-coated quantum dots (Qtracker 655, Quantum Dot Corporation, Hayward, CA) were injected with the same excitation to visualize blood flow. To create time-lapse sequences, we typically scanned 50×400×400 μm volumes of tissue at 3 μm Z-steps and 30 second intervals.

Data analysis

Cell movement was analyzed with Volocity software (Improvision). To calculate cell speeds, the coordinates of each cell were calculated and tracked over time, and motility parameters were calculated. Average cell velocity was calculated as described previously[10]. Cells were characterized as immobile if their average velocity was less than 2 μm/min. The arrest coefficient was calculated as the percentage of each track in which the cell moved more slowly than 2 μm/min[6]. The turning angle is the absolute angle between the velocity vectors before and after a measurement time point[7]. The confinement index is calculated as the ratio of maximum displacement to path length[6]. Multivariate ANOVA was conducted to assess statistical significance, and planned contrasts were used to assess differences between individual conditions when appropriate. *p* values smaller than 0.05 were considered significant.

Acknowledgements

We thank R. Steinman for discussions, E. Besmer for help with the manuscript, W. Gan for guidance on two-photon microscopy, S. Boscardin for α-DEC-CSP and R. Masalimani for α-DEC-OVA plasmid. Supported by NIH grants AI055037 (M.L.D.) and AI051573 (M.C.N.), the Irene Diamond Foundation (M.L.D.), and the Howard Hughes Medical Institute (M.C.N.). G.S. was supported in part by a post-doctoral fellowship from the Rothschild Foundation; R.L.L. was supported by MSTP grant GM07739; D.D. was supported by the German Research Foundation DU 548/1-1.

NIH-PA Author Manuscript

NIH-PA Author Manuscript

NIH-PA Author Manuscript

References

1. Stoll S, Delon J, Brotz TM, Germain RN. Dynamic imaging of T cell-dendritic cell interactions in lymph nodes. Science 2002;296:1873–6. [PubMed: 12052961]
2. Miller MJ, Wei SH, Parker I, Cahalan MD. Two-Photon Imaging of Lymphocyte Motility and Antigen Response in Intact Lymph Node. Science 2002;296:1869–1873. [PubMed: 12016203]
3. Bousso P, Robey E. Dynamics of CD8+ T cell priming by dendritic cells in intact lymph nodes. Nat Immunol 2003;4:579–85. [PubMed: 12730692]
4. Miller MJ, Hejazi AS, Wei SH, Cahalan MD, Parker I. T cell repertoire scanning is promoted by dynamic dendritic cell behavior and random T cell motility in the lymph node. Proc Natl Acad Sci U S A 2004;101:998–1003. [PubMed: 14722354]
5. Miller MJ, Safrina O, Parker I, Cahalan MD. Imaging the Single Cell Dynamics of CD4+ T Cell Activation by Dendritic Cells in Lymph Nodes. J Exp Med 2004;200:847–56. [PubMed: 15466619]
6. Hugues S, et al. Distinct T cell dynamics in lymph nodes during the induction of tolerance and immunity. Nat Immunol 2004;5:1235–42. [PubMed: 15516925]
7. Mempel TR, Henrickson SE, Von Andrian UH. T-cell priming by dendritic cells in lymph nodes occurs in three distinct phases. Nature 2004;427:154–9. [PubMed: 14712275]
8. Miller, M.J., Wei, S.H., Cahalan, M.D. & Parker, I. Autonomous T cell trafficking examined in vivo with intravital two-photon microscopy. *Proc. Natl. Acad. Sci. U. S. A.* (2003).
9. Gunzer, M. et al. A spectrum of biophysical interaction modes between T cells and different antigen presenting cells during priming in 3-D collagen and in vivo. *Blood* (2004).
10. Lindquist RL, et al. Visualizing dendritic cell networks in vivo. Nat Immunol 2004;5:1243–50. [PubMed: 15543150]
11. Banchereau J, Pascual V, Palucka KA. Autoimunity through cytokine-induced dendritic cell activation. Immunity 2004;20:539–550. [PubMed: 15142523]
12. Guermonprez P, Valladeau J, Zitvogel L, Thery C, Amigorena S. Antigen presentation and T cell stimulation by dendritic cells. Annu Rev Immunol 2002;20:621–67. [PubMed: 11861614]
13. Lanzavecchia A, Sallusto F. Regulation of T cell immunity by dendritic cells. Cell 2001;106:263–6. [PubMed: 11509174]
14. Liu YJ. Dendritic cell subsets and lineages, and their functions in innate and adaptive immunity. Cell 2001;106:259–62. [PubMed: 11509173]
15. Mellman I, Steinman RM. Dendritic cells: specialized and regulated antigen processing machines. Cell 2001;106:255–8. [PubMed: 11509172]
16. Steinman RM, Hawiger D, Nussenzweig MC. Tolerogenic dendritic cells. Annu Rev Immunol 2003;21:685–711. [PubMed: 12615891]
17. Belz GT, et al. The CD8alpha(+) dendritic cell is responsible for inducing peripheral self-tolerance to tissue-associated antigens. J Exp Med 2002;196:1099–104. [PubMed: 12391021]
18. Huang FP, et al. A discrete subpopulation of dendritic cells transports apoptotic intestinal epithelial cells to T cell areas of mesenteric lymph nodes. J Exp Med 2000;191:435–44. [PubMed: 10662789]
19. Inaba K, et al. Efficient presentation of phagocytosed cellular fragments on the major histocompatibility complex class II products of dendritic cells. J Exp Med 1998;188:2163–73. [PubMed: 9841929]
20. Iyoda T, et al. The CD8+ dendritic cell subset selectively endocytoses dying cells in culture and in vivo. J Exp Med 2002;195:1289–302. [PubMed: 12021309]
21. Liu K, et al. Immune tolerance after delivery of dying cells to dendritic cells in situ. J Exp Med 2002;196:1091–7. [PubMed: 12391020]
22. Scheinecker C, McHugh R, Shevach EM, Germain RN. Constitutive presentation of a natural tissue autoantigen exclusively by dendritic cells in the draining lymph node. J Exp Med 2002;196:1079–90. [PubMed: 12391019]
23. Hawiger D, et al. Dendritic cells induce peripheral T cell unresponsiveness under steady state conditions in vivo. J Exp Med 2001;194:769–79. [PubMed: 11560993]

NIH-PA Author Manuscript

NIH-PA Author Manuscript

NIH-PA Author Manuscript

24. Bonifaz L, et al. Efficient targeting of protein antigen to the dendritic cell receptor DEC-205 in the steady state leads to antigen presentation on major histocompatibility complex class I products and peripheral CD8+ T cell tolerance. J Exp Med 2002;196:1627–38. [PubMed: 12486105]
25. Probst HC, Lagnel J, Kollias G, van den Broek M. Inducible transgenic mice reveal resting dendritic cells as potent inducers of CD8+ T cell tolerance. Immunity 2003;18:713–20. [PubMed: 12753747]
26. Brimnes MK, Bonifaz L, Steinman RM, Moran TM. Influenza virus-induced dendritic cell maturation is associated with the induction of strong T cell immunity to a coadministered, normally nonimmunogenic protein. J Exp Med 2003;198:133–44. [PubMed: 12847140]
27. Hawiger D, Masilamani R, Betelli E, Kuchroo VJ, Nussenzweig MC. Immunological Unresponsiveness Characterized by Increased Expression of CD5 on Peripheral T cells Induced by Dendritic Cells In Vivo. Immunity 2004;20:695–705. [PubMed: 15189735]
28. Kurts C, Kosaka H, Carbone FR, Miller JF, Heath WR. Class I-restricted cross-presentation of exogenous self-antigens leads to deletion of autoreactive CD8(+) T cells. J Exp Med 1997;186:239–45. [PubMed: 9221753]
29. Zal T, Volkmann A, Stockinger B. Mechanisms of tolerance induction in major histocompatibility complex class II-restricted T cells specific for a blood-borne self-antigen. J Exp Med 1994;180:2089–99. [PubMed: 7964486]
30. Bonifaz LC, et al. In vivo targeting of antigens to maturing dendritic cells via the DEC-205 receptor improves T cell vaccination. J Exp Med 2004;199:815–24. [PubMed: 15024047]
31. Kearney ER, Pape KA, Loh DY, Jenkins MK. Visualization of peptide-specific T cell immunity and peripheral tolerance induction in vivo. Immunity 1994;1:327–39. [PubMed: 7889419]
32. Van Parijs L, Peterson DA, Abbas AK. The Fas/Fas ligand pathway and Bcl-2 regulate T cell responses to model self and foreign antigens. Immunity 1998;8:265–74. [PubMed: 9492007]
33. Redmond WL, Hernandez J, Sherman LA. Deletion of naive CD8 T cells requires persistent antigen and is not programmed by an initial signal from the tolerogenic APC. J Immunol 2003;171:6349–54. [PubMed: 14662832]
34. Barnden MJ, Allison J, Heath WR, Carbone FR. Defective TCR expression in transgenic mice constructed using cDNA-based alpha- and beta-chain genes under the control of heterologous regulatory elements. Immunol Cell Biol 1998;76:34–40. [PubMed: 9553774]
35. Huang AY, Qi H, Germain RN. Illuminating the landscape of in vivo immunity: insights from dynamic in situ imaging of secondary lymphoid tissues. Immunity 2004;21:331–9. [PubMed: 15357944]
36. Sumen C, Mempel TR, Mazo IB, von Andrian UH. Intravital microscopy: visualizing immunity in context. Immunity 2004;21:315–29. [PubMed: 15357943]
37. Bajenoff M, Granjeaud S, Guerder S. The strategy of T cell antigen-presenting cell encounter in antigen-draining lymph nodes revealed by imaging of initial T cell activation. J Exp Med 2003;198:715–24. [PubMed: 12953093]
38. Negulescu PA, Krasieva TB, Khan A, Kerschbaum HH, Cahalan MD. Polarity of T cell shape, motility, and sensitivity to antigen. Immunity 1996;4:421–30. [PubMed: 8630728]
39. Dustin ML, Bromley SK, Kan Z, Peterson DA, Unanue ER. Antigen receptor engagement delivers a stop signal to migrating T lymphocytes. Proc Natl Acad Sci USA 1997;94:3909–3913. [PubMed: 9108078]
40. Ohl L, et al. CCR7 governs skin dendritic cell migration under inflammatory and steady-state conditions. Immunity 2004;21:279–88. [PubMed: 15308107]
41. Benvenuti F, et al. Dendritic cell maturation controls adhesion, synapse formation, and the duration of the interactions with naive T lymphocytes. J Immunol 2004;172:292–301. [PubMed: 14688337]
42. Wulfing C, et al. Costimulation and endogenous MHC ligands contribute to T cell recognition. Nat Immunol 2002;3:42–7. [PubMed: 11731799]
43. Huppa JB, Gleimer M, Sumen C, Davis MM. Continuous T cell receptor signaling required for synapse maintenance and full effector potential. Nat Immunol 2003;4:749–55. [PubMed: 12858171]
44. Valitutti S, Muller S, Cella M, Padovan E, Lanzavecchia A. Serial triggering of many T-cell receptors by a few peptide-MHC complexes. Nature 1995;375:148–51. [PubMed: 7753171]
45. Itano AA, et al. Distinct dendritic cell populations sequentially present antigen to CD4 T cells and stimulate different aspects of cell-mediated immunity. Immunity 2003;19:47–57. [PubMed: 12871638]

NIH-PA Author Manuscript

NIH-PA Author Manuscript

NIH-PA Author Manuscript

46. Kang YS, et al. SIGN-R1, a novel C-type lectin expressed by marginal zone macrophages in spleen, mediates uptake of the polysaccharide dextran. Int Immunol 2003;15:177–86. [PubMed: 12578847]

47. Wright DE, et al. Cyclophosphamide/granulocyte colony-stimulating factor causes selective mobilization of bone marrow hematopoietic stem cells into the blood after M phase of the cell cycle. Blood 2001;97:2278–2285. [PubMed: 11290588]

48. Hadjantonakis AK, Macmaster S, Nagy A. Embryonic stem cells and mice expressing different GFP variants for multiple non-invasive reporter usage within a single animal. BMC Biotechnol 2002;2:11. [PubMed: 12079497]

NIH-PA Author Manuscript
NIH-PA Author Manuscript
NIH-PA Author Manuscript

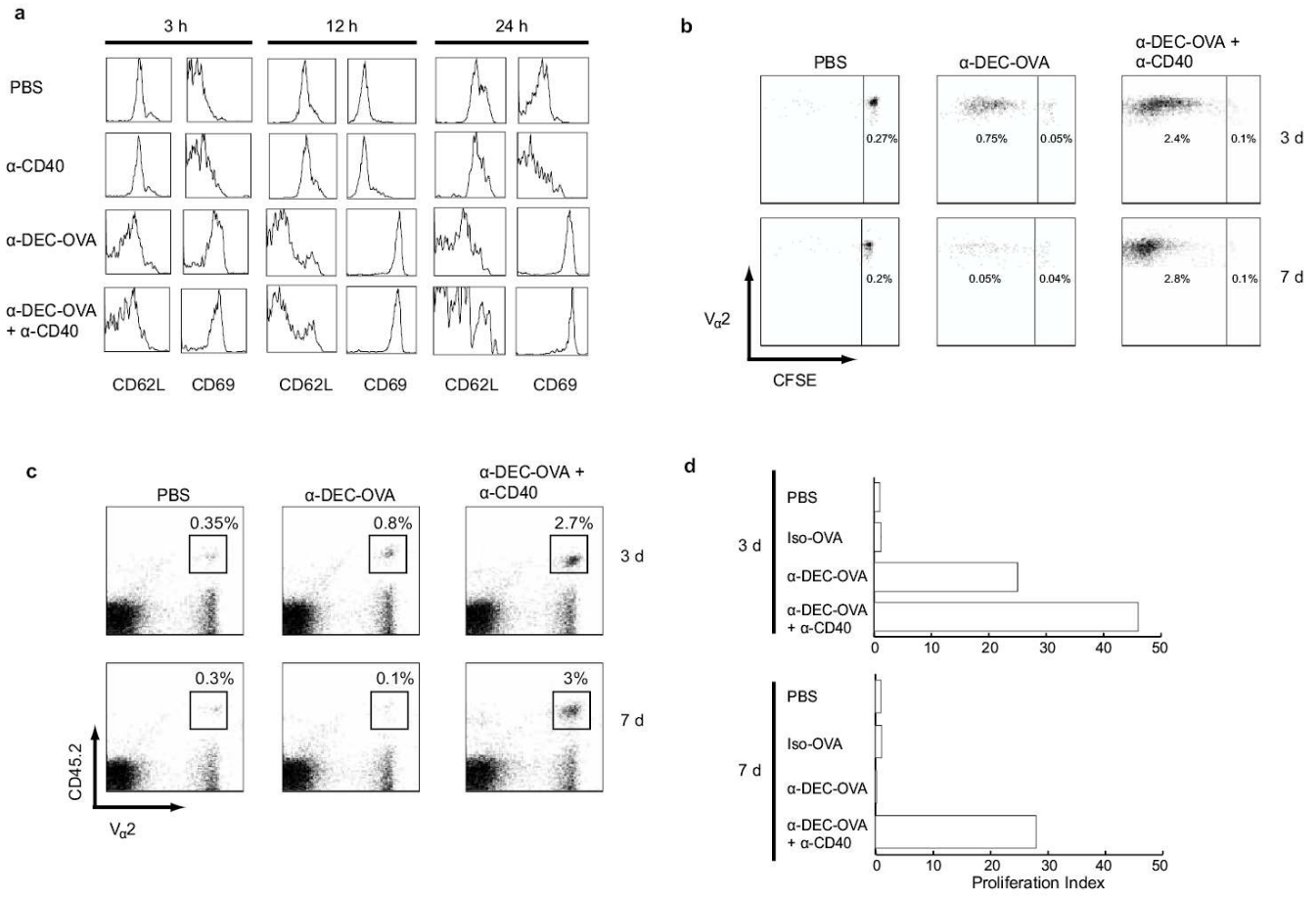

Figure 1.

OT-II T cell activation and tolerance induced by α-DEC-OVA. Transferred OT-II T cells (CD45.2) divide in response to antigen presented by DCs *in vivo* by day 3 and are deleted in the absence of α-CD40 by day 7. (**a**) Similar activation of OT-II T cells after delivery of α-DEC-OVA with and without α-CD40. Histograms show surface expression of the indicated marker gated on CD45.2$^+$ TCR V$_\alpha$2$^+$ cells 3, 12, and 24 h after challenge (see Methods). (**b**) Plots show CFSE dye dilution of gated populations of CD4$^+$ CD45.2$^+$ T cells 3 and 7 days after challenge with 2 μg of α-DEC-OVA with or without α-CD40 or with PBS. Percentages of CFSE$^{hi/lo}$ TCR V$_\alpha$2$^+$ cells out of CD4$^+$ T cells are indicated. (**c**) Numbers of surviving OT-II cells 3 or 7 days after challenge as in **b**; percentages of CD45.2$^+$ TCR V$_\alpha$2$^+$ cells among CD4$^+$ T cells are indicated. Antigen-specific T cells were deleted unless CD40 was engaged. (**d**) OT-II cells are only transiently activated by *in vivo* delivery of α-DEC-OVA to DCs. CD4$^+$ cells were purified from peripheral lymph nodes 3 or 7 days after challenge as in **b** and cultured with irradiated CD11c$^+$ cells in the presence or absence of OVA peptide; proliferation index denotes the ratio of thymidine incorporation in antigen-challenged to unchallenged cells, corrected for background proliferation. Data are representative of 3 to 4 experiments.

NIH-PA Author Manuscript
NIH-PA Author Manuscript
NIH-PA Author Manuscript

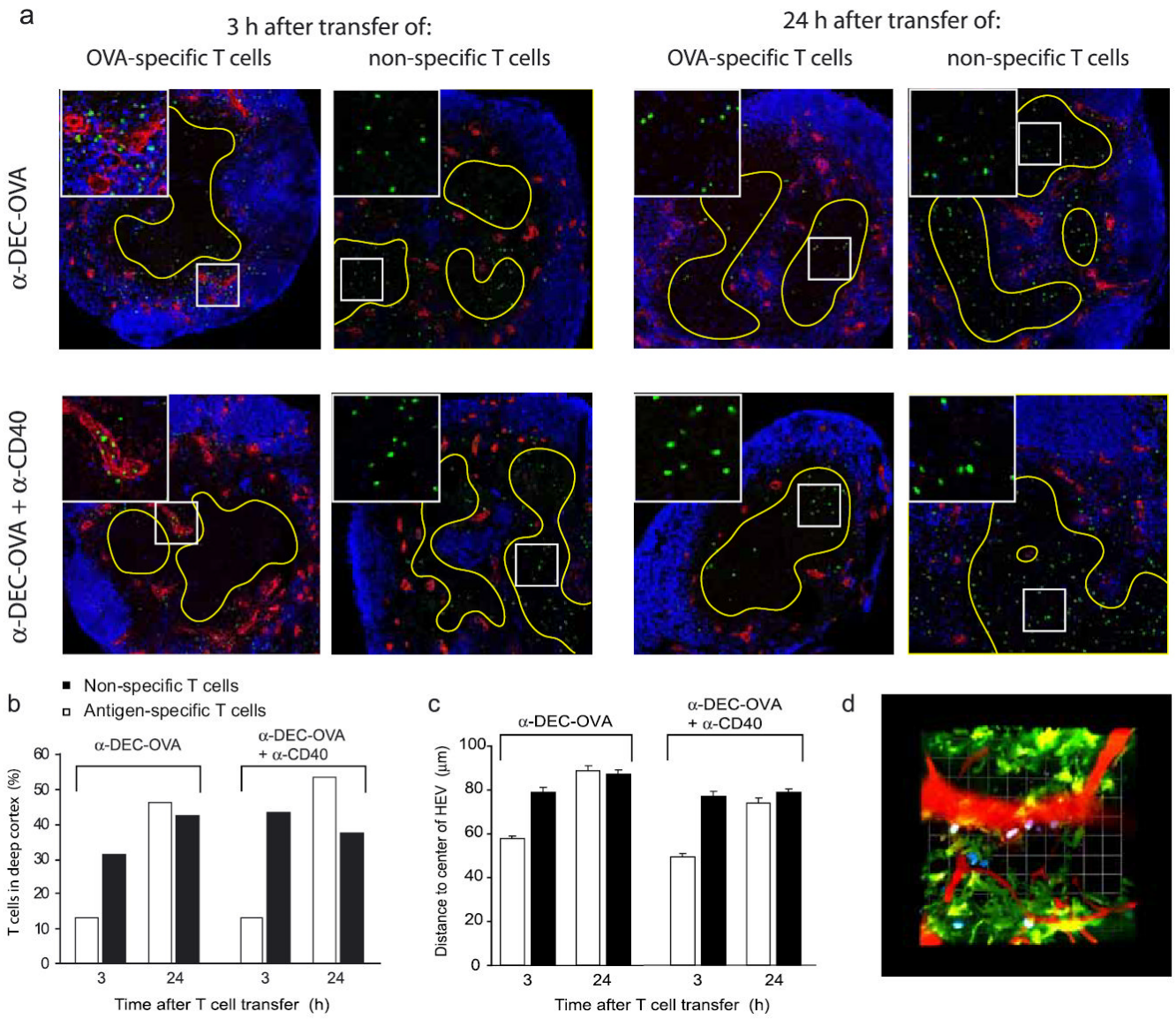

Figure 2.

During early stages of priming and tolerance, antigen-specific T cells are located closer to HEVs in the superficial paracortex than non-specific T cells. (**a**) Confocal micrographs of lymph node frozen sections immunostained for MECA-79 (red) and B220 (blue); EGFP fluorescence from transferred T cells (green) was visualized directly. EGFP-expressing OT-II or non-TCR transgenic T cells were transferred into C57BL/6 mice five h after injection of α-DEC-OVA with or without α-CD40. Insets show high-magnification view of T cells near HEVs. (left panels) or in the deep paracortex (right panels); the deep paracortex is outlined in yellow. Optical sections were 1.2 μm in both MECA-79 and B220 channels and 5 mm in the EGFP channel. (**b**) The percentage of T cells in the deep paracortex was calculated as described previously[37]. Three h after cell transfer, there were more non-specific T cells found in the deep paracortex than antigen-specific T cells; at 24 h after cell transfer, specific and non-specific T cells were more equally represented in the deep paracortex. (**c**) The distance from T cells to the nearest HEV. Three h after cell transfer, antigen-specific cells were closer than non-specific cells to HEVs. (**d**) Two-photon visualization of specific and non-specific T cells near an HEV

in the inguinal lymph node of an anesthetized mouse. Error bars denote standard error of the mean. Asterisks indicate significant differences; see text for p values. Data are representative of 3 experiments.

NIH-PA Author Manuscript
NIH-PA Author Manuscript
NIH-PA Author Manuscript

NIH-PA Author Manuscript
NIH-PA Author Manuscript
NIH-PA Author Manuscript

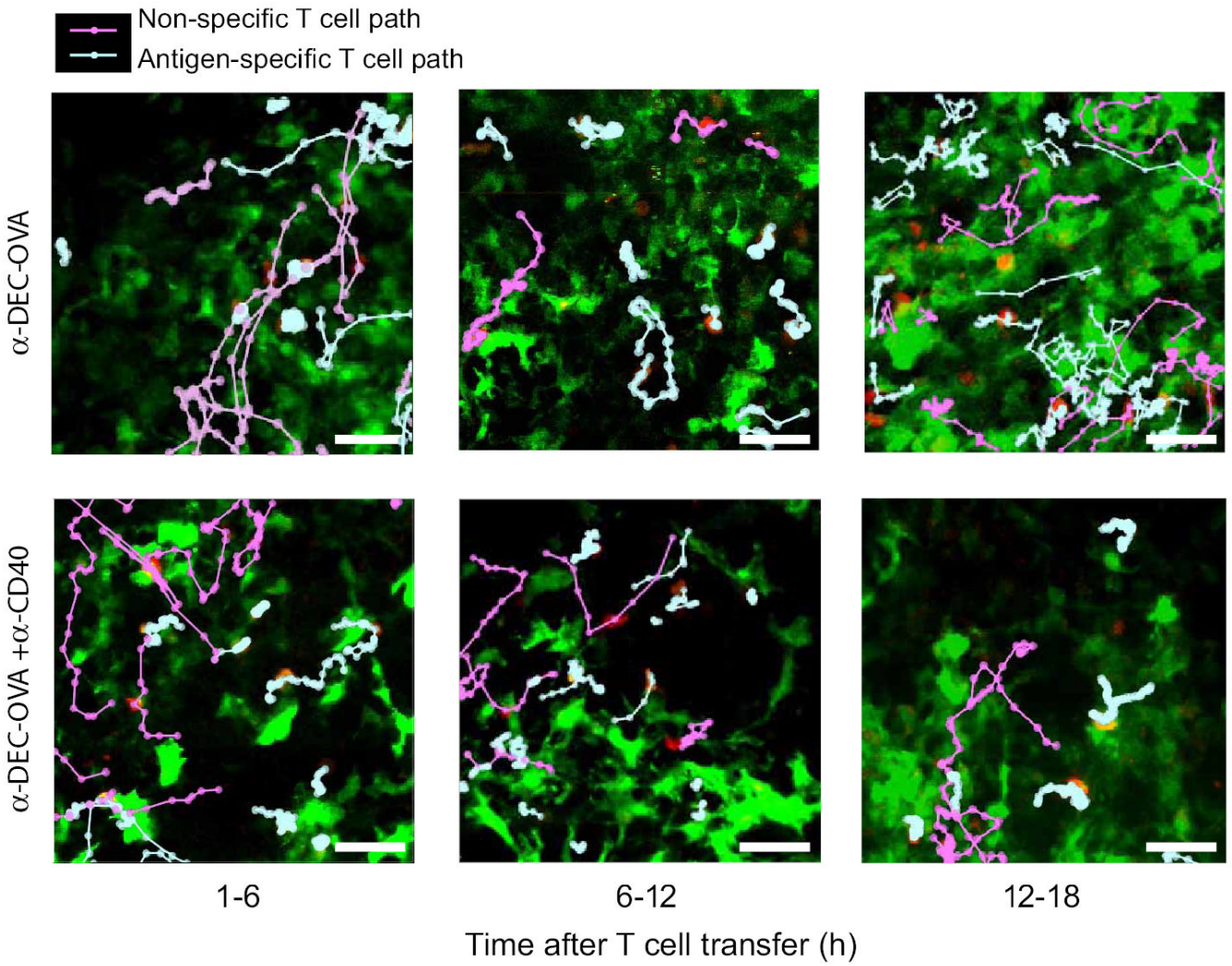

Figure 3.

Tracking of specific and non-specific T cells in the lymph nodes of living mice. Representative tracks of EGFP-OT-II T cells and ECFP-T cells. Antigen-specific EGFP-OT-II cells and non-specific ECFP-T cells were tracked throughout the imaged volume for the duration of imaging, and the XY projection of their tracks is displayed. Data representative of a total of 62 imaging fields analyzed.

NIH-PA Author Manuscript

NIH-PA Author Manuscript

NIH-PA Author Manuscript

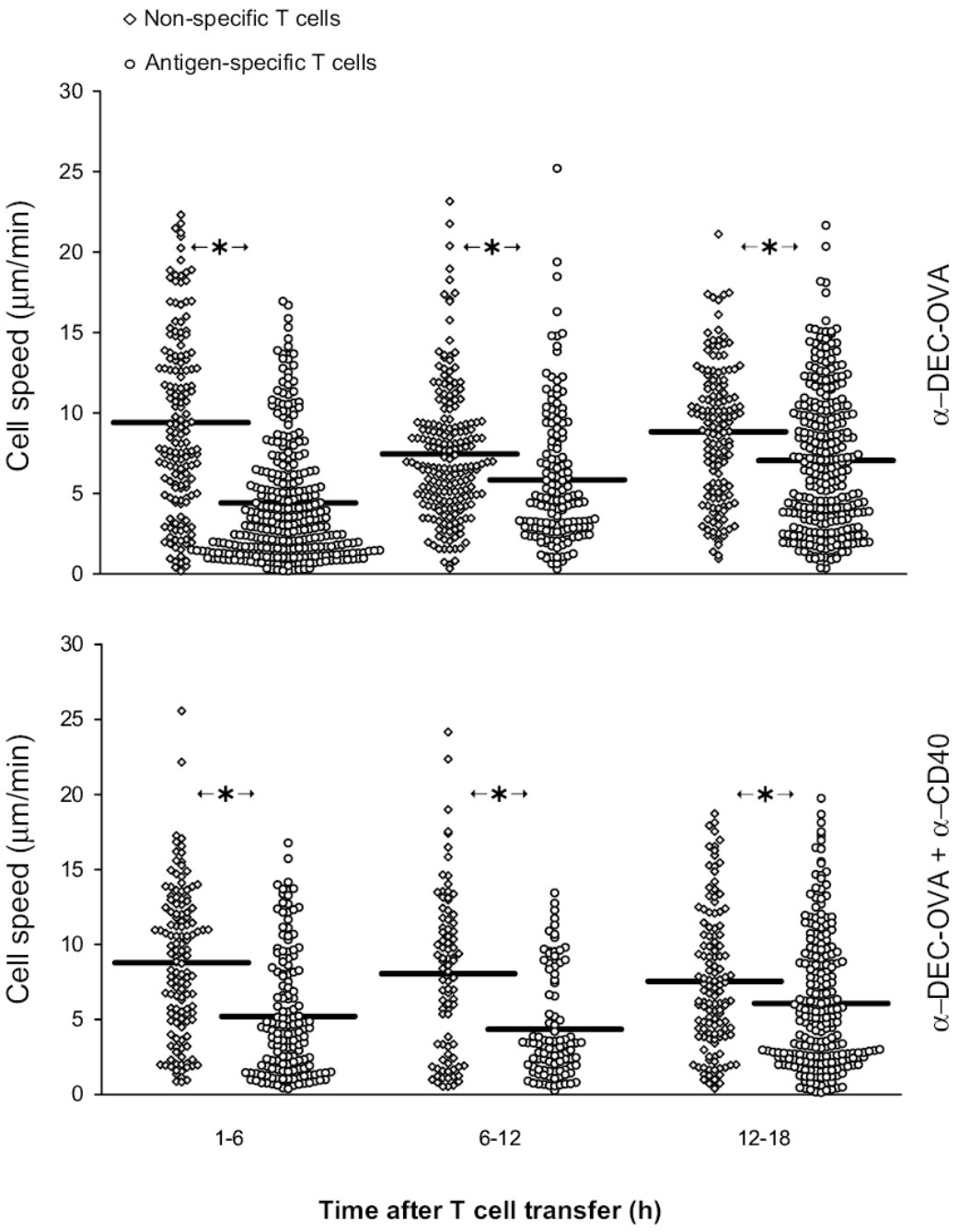

Figure 4.

Mean cell velocities in tolerizing and priming conditions. Mice were injected with antibodies and T cells, inguinal lymph nodes were imaged, and specific and non-specific T cells were tracked as above. Antigen-specific EGFP-OT-II cells move slowly at 1–5 h in both priming (mean cell velocity 5.2 μm/min) and tolerance (4.4 μm/min), while non-specific T cells maintain their normal velocity of ~9 μm/min. Error bars denote standard error of the mean. Asterisks indicate significant differences; see text for *p* values. Plot summarizes collective data from all experiments.

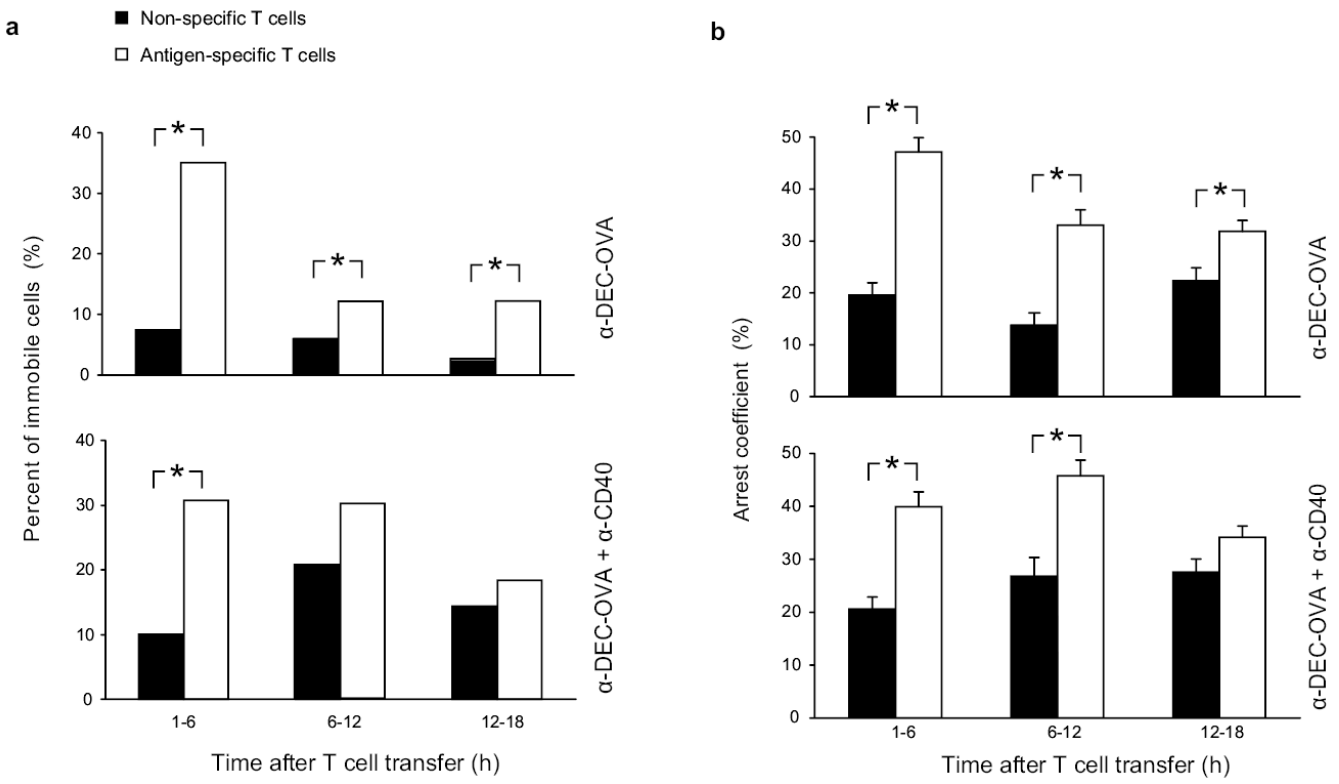

Figure 5.

Early T cell arrest in tolerizing and priming conditions. (**a**) Percent of immobile cells in priming and tolerance. More antigen-specific EGFP-OT-II cells than non-specific T cells are immobile (mean velocity <2 μm/min) at 1–6 h in both priming and tolerance. (**b**) Arrest coefficient of specific and non-specific T cells. The arrest coefficient is the percentage of each track that a cell is immobile (instantaneous velocity <2 μm/min). In both priming and tolerance, from 1–6 h after T cell transfer, EGFP-OT-II cells are arrested for an average of 40–50% of each track, as compared to 20% for non-specific T cells. Error bars denote standard error of the mean. Asterisks indicate significant differences; see text for *p* values. Graphs summarize collective data from all experiments.

NIH-PA Author Manuscript
NIH-PA Author Manuscript
NIH-PA Author Manuscript

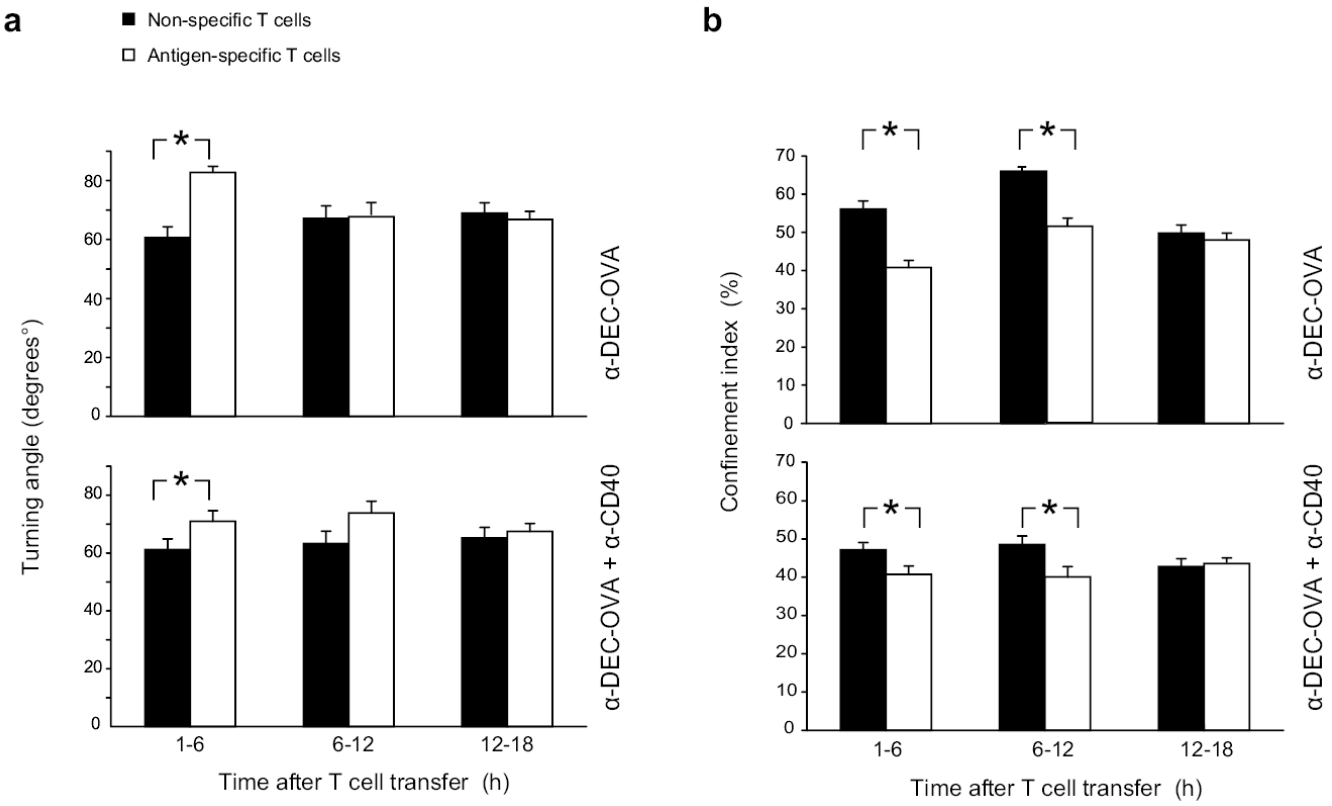

Figure 6.

Directionality of specific and non-specific T cells. (**a**) Turning angle of specific and non-specific T cells. Lower turning angles indicate more linear cell movement. (**b**) Confinement index of specific and non-specific T cells. Confinement index is the ratio of the maximum cell displacement to the path length; a higher confinement index indicates more linear movement. At time points when antigen-specific cells move more slowly than non-specific cells, the non-specific cells move more linearly by both measures of directionality. Graphs summarize collective data from all experiments. Error bars denote standard error of the mean. Asterisks indicate significant differences; see text for *p* values.

NIH-PA Author Manuscript
NIH-PA Author Manuscript
NIH-PA Author Manuscript

NIH-PA Author Manuscript
NIH-PA Author Manuscript
NIH-PA Author Manuscript

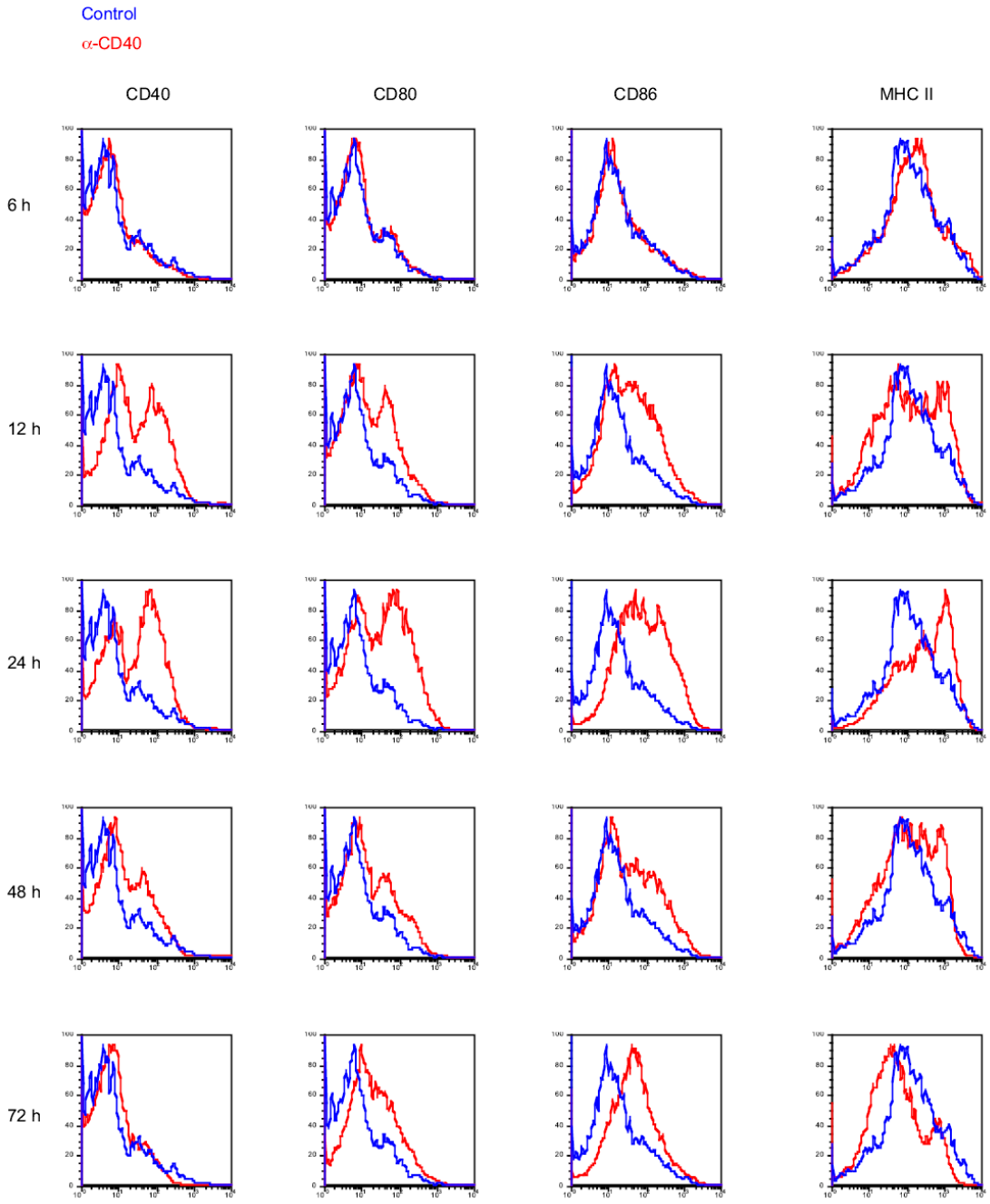

Supplementary Figure 1.

DC maturation induced by α-CD40 antibody. Mice were injected i.p. with 50 μg α-CD40, lymph nodes were harvested at the indicated times, and $CD11c^+$ DCs were isolated by immunomagnetic selection and analyzed by flow cytometry. Histograms show the indicated surface marker, gated on $CD11c^+$ $CD3^-$ $CD19^-$ cells. Data representative of 2 separate experiments.

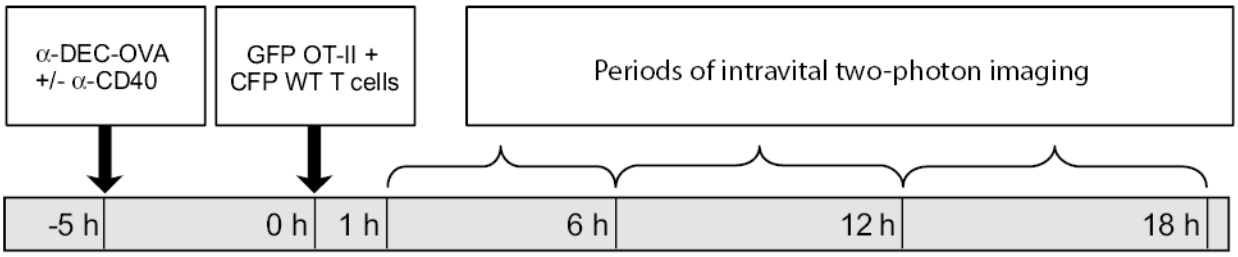

Supplementary Figure 2.
Timeline for imaging T cell tolerance and priming. CD11c-EYFP mice were injected with α-DEC-OVA with or without α-CD40 5 h prior to transfer of EGFP-OT-II cells and wild-type ECFP-T cells; inguinal lymph nodes were imaged intravitally at the indicated periods.

NIH-PA Author Manuscript
NIH-PA Author Manuscript
NIH-PA Author Manuscript

NIH-PA Author Manuscript
NIH-PA Author Manuscript
NIH-PA Author Manuscript

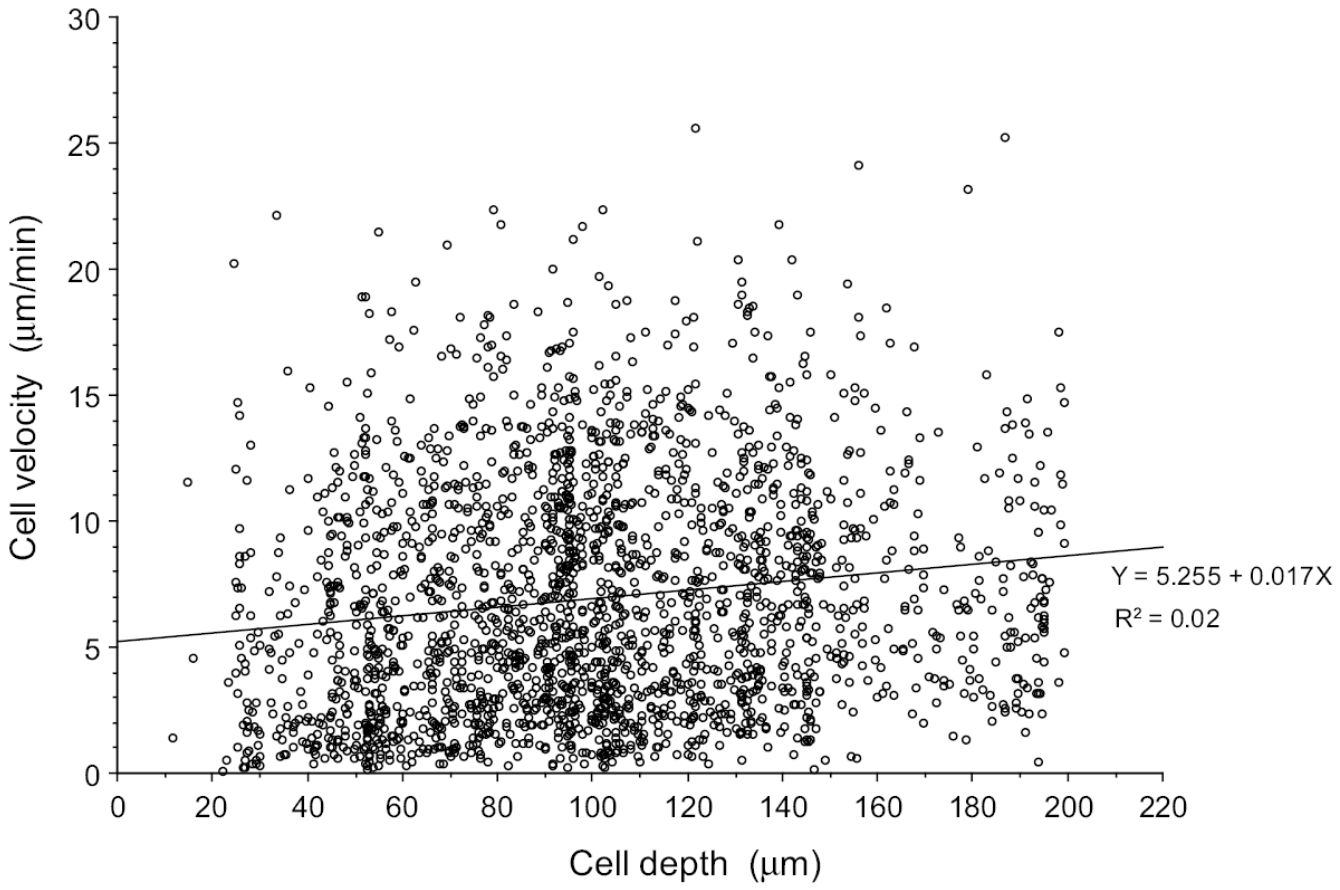

Supplementary Figure 3.
There is no systematic association between cell depth and average cell speed. The depth of each cell was calculated from its depth in the imaging field and the depth of the imaging field below the lymph node capsule. Plot summarizes collective data from all experiments.

NIH-PA Author Manuscript
NIH-PA Author Manuscript
NIH-PA Author Manuscript

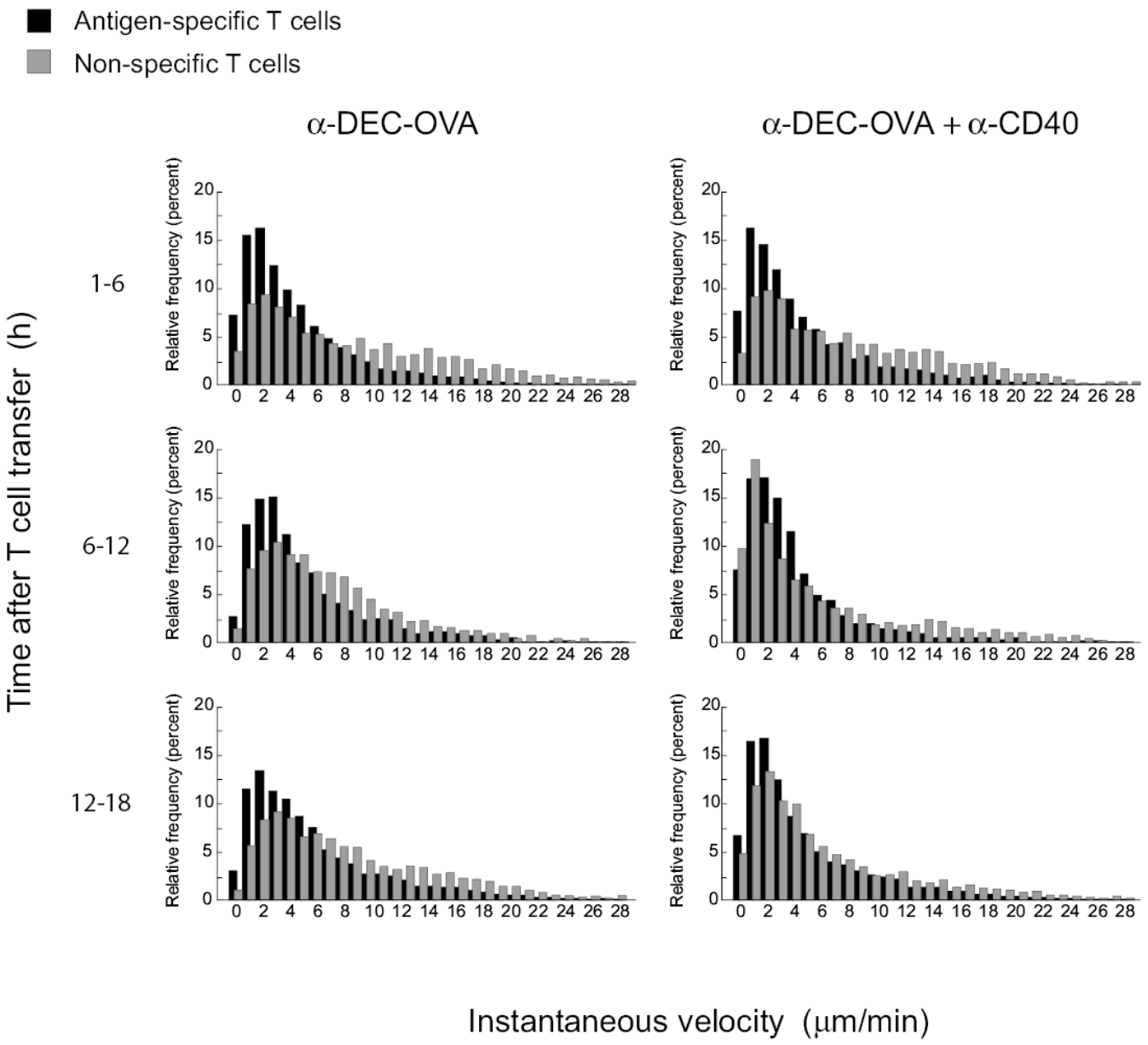

Supplementary Figure 4.
Instantaneous velocities of specific and non-specific cells. Results are similar to those obtained for mean cell velocity. Histogram summarizes collective data from all experiments. Error bars denote standard error of the mean. Asterisks indicate significant differences.

NIH-PA Author Manuscript
NIH-PA Author Manuscript
NIH-PA Author Manuscript

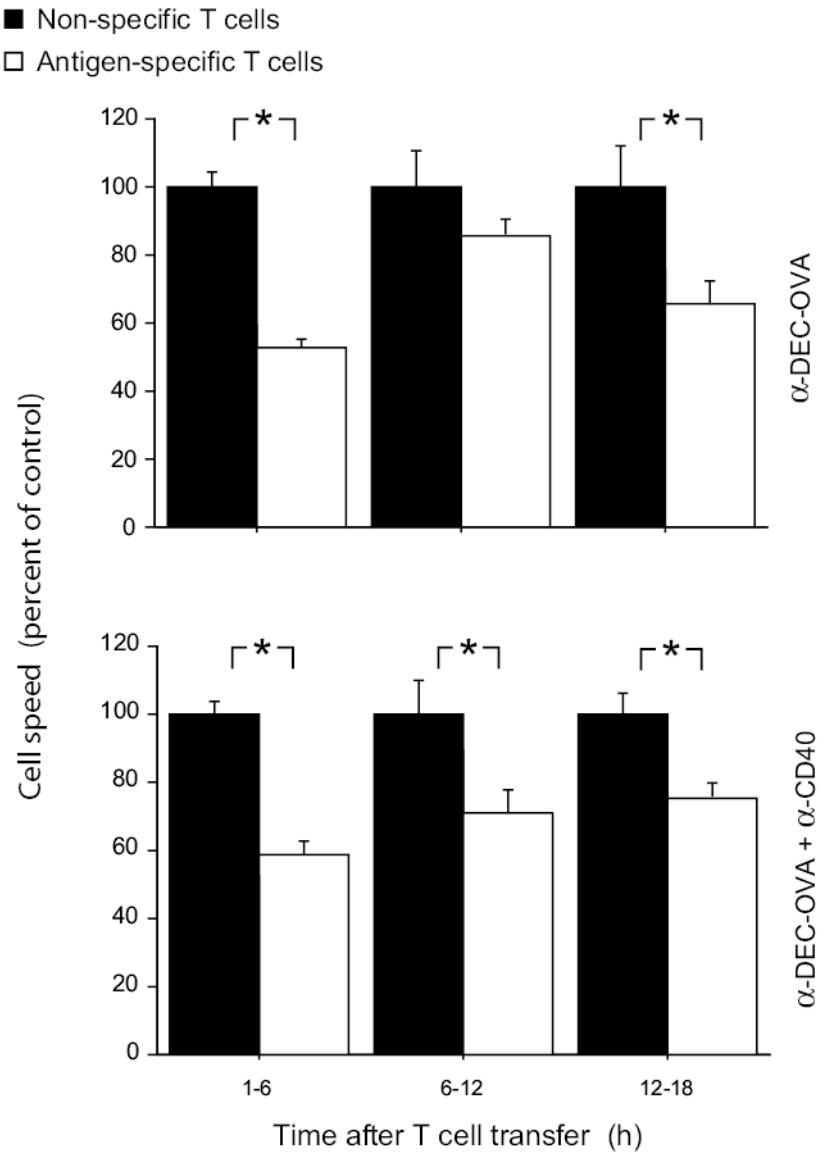

Supplementary Figure 5.

Speeds of antigen-specific cells normalized to speed of control cells in the same imaging field. Cells were transferred, imaged, and tracked as above, and the median speed of the non-specific cells was determined for each imaging field; fields with fewer than three non-specific cells were excluded. Antigen-specific cell speeds were expressed as a percentage of the median non-specific speed in the same field. Chart summarizes collective data from all experiments. Results are similar to those obtained for mean cell velocity.